JOURNAL OF COMPUTATIONAL PHYSICS 38, 294–326 (1980)

Finite Difference Solution of the Cosserat Fluid Jet Equations

D.B. BOGY

Department of Mechanical Engineering, University of California, Berkeley, California 94720

S. J. SHINE

Department of Mechanical Engineering, University of Dar-es-Salaam, Dar-es-Salaam, Tanzania

AND

F. E. TALKE

IBM Research Laboratory, San Jose, California 95114

Received August 9, 1979

A simultaneous finite difference solution of the nonlinear Cosserat fluid jet equations for a semi-infinite jet emanating from a circular nozzle is presented. The problem is treated as time-dependent with a small amplitude periodic excitation of the velocity at the nozzle. Solutions for the jet radius and velocity are computed up to the breakoff point where the radius becomes zero or the absolute value of the velocity exceeds a chosen maximum value. It is found that when the dimensionless frequency of the excitation, ω, satisfies $\omega < 1$, the disturbance wave grows in amplitude as it propagates downstream until it finally breaks the jet. The breakoff point depends on the frequency and amplitude of the excitation, the jet velocity, and the viscosity of the fluid. When $\omega > 1$ the disturbance is stable and therefore no jet breakup occurs. Even for the unstable frequencies high viscocity can appreciably dampen the growth of the disturbance. For $\omega < 1$ and low viscosity the jet breaks up into main drops of twice the nozzle diameter and for certain conditions, small, so-called satellite drops are shown to form between the main drops. The results are compared with results from perturbation solutions of the same equations due to Bogy [*IBM J. Res. Develop.* **23** No. 1 (1979), 87–92; *Phys. Fluids* **22**, No. 2 (1979), 224–230; *J. Appl. Mech.* **45** (1978), 469–474].

1. INTRODUCTION

The Cosserat fluid jet equations derived by Green *et al.* [6] and Green [7] have been studied by Bogy [1–5] and Caulk and Naghdi [19, 21]. The perturbation solutions [2, 3] provide a useful guide to this work, where our purpose is to present a finite difference (FD) solution of the one-dimensional nonlinear Cosserat jet equations given in Green [7] for a viscous fluid with surface tension.

0021-9991/80/150294–33$02.00/0

The FD solution of these equations is not easy. In fact the computational effort is quite large if we hope to accurately predict the jet breakoff point and drop formation, since we have to use a very fine space-time mesh. Thus the mesh step in the direction of the jet must be extremely small compared to the length of the column of liquid from the nozzle to the breakoff point. The problem is further compounded by the presence of space derivatives of up to fourth order and mixed derivatives of up to third order. Furthermore we have to deal with a singular region at the jet breakoff point, where the radius goes to zero and the velocity and certain derivatives become very large.

It is well known in numerical analysis that one of the least obvious tasks in FD methods is the introduction of the additional boundary and/or initial conditions which have to be added into some schemes to render them executable. Also difficult is the treatment of singular points, such as corners, crack tips, and in this case the jet breakoff point. Ilan [10] discusses these tasks in connection with FD schemes for the problem of elastic wave propagation in a quarter plane, where a corner singularity and additional boundary conditions are treated. Because of the high order difference equations required to get suitable solutions more information is required at the nozzle and downstream than the known boundary conditions produce for the problem. As will be discussed later we resolved this by making use of results from the perturbation solution of the same equations due to Bogy [2] or by making some reasonable assumptions.

Guided by results from preliminary schemes we had to derive higher-order accurate schemes to deal with the singular region near the jet breakoff point. Recently a high-accuracy compact FD technique has been used [12–15] in the solution of PDEs in which higher spatial accuracy is achieved without using more grid points. The technique introduced by Kreiss (see Orszag and Israel [15]) treats functions and their derivatives as unknowns at the grid points and results in a lower matrix system to solve, e.g., a tridiagonal system instead of a pentadiagonal system for the same accuracy. However, this technique works well only with explicit schemes and where no mixed derivatives are involved. When used with implicit schemes for improved stability a block tridiagonal system results, which may not be easier or less time consuming than the equivalent pentadiagonal system it replaces (see Hirsh [12]). Because of the complexity of our equations and the presence of mixed derivatives we obtained higher spatial accuracy by the traditional approach of taking more grid points to approximate the derivatives and solving pentadiagonal and heptadiagonal matrix equations.

Time-dependent computational techniques for inviscid flows have been the subject of many research papers. It is now generally accepted that such techniques can work very well as long as the flow is continuous. However, in problems of practical interest discontinuities and singularities do exist and are in fact often the most interesting features of the flow. In such problems it is often useful to introduce artificial viscosity to smear out discontinuities, as explained by Moretti and Salas [16]. In the same reference they discuss the use of real and artificial viscosity from a numerical standpoint. Here both inviscid and viscous schemes are investigated.

In the simultaneous FD solution of the Cosserat equations we were faced with difficulties with computer memory requirements and costs. One of the equations is numerically very cumbersome since it has 17 terms, some of them with high and mixed derivatives. For the case of a fast jet (large Weber number) with a very small perturbation amplitude of the velocity at the nozzle, the breakoff point is relatively far downstream. Since the disturbance grows downstream from the nozzle a long jet must be finely discretized; and since the disturbance is periodic in time the computation has to be carried out for many cycles of the input excitation at a very small time step. Thus with this fine space-time mesh required for a good solution we can easily use up the entire core memory of most machines with CPU time running to several minutes. However, for conditions under which the jet breaks up near the nozzle good solutions can be obtained in a very short CPU time.

As will be discussed in a later section, stability analyses for high order PDEs of complicated form are very difficult and are usually not carried out. Instead, FD schemes consistent with the PDEs are derived and conditions for which they are stable are determined by numerical experimentation.

2. The Cosserat Fluid Jet Equations

The straight circular jet equations presented in Green [7] were written in terms of dimensionless radius $\phi(z, t)$ and axial velocity $v(z, t)$ (z and t are the dimensionless axial coordinate and time) in Bogy [1] as

$$\begin{aligned} 2\phi\phi_t + 2\phi\phi_z v + \phi^2 v_z &= 0, \\ v_t + vv_z - \tfrac{1}{2}\phi\phi_z(v_{zt} + vv_{zz} - \tfrac{1}{2}v_z^2) - \tfrac{1}{8}\phi^2(v_{zzt} + vv_{zzz}) &= X + Y, \end{aligned} \tag{1}$$

where X and Y represent the surface tension and viscosity terms, respectively, and have the forms

$$\begin{aligned} X &= \frac{1}{W}\left\{\frac{\phi_z}{\phi^2(1+\phi_z^2)^{1/2}} + \frac{\phi_z\phi_{zz}}{\phi(1+\phi_z^2)^{3/2}} + \frac{\phi_{zzz}}{(1+\phi_z^2)^{3/2}} - \frac{3\phi_z\phi_{zz}^2}{(1+\phi_z^2)^{5/2}}\right\}, \\ Y &= \frac{1}{R}\left\{\frac{6\phi_z v_z}{\phi} + v_{zz}\left(3 - \frac{3}{2}\phi_z^2 - \frac{1}{2}\phi\phi_{zz}\right) - \phi\phi_z v_{zzz} - \frac{\phi^2}{8}v_{zzzz}\right\}, \end{aligned} \tag{2}$$

in which W and R represent the Weber and Reynolds numbers given by

$$W = \frac{\rho a v_0^2}{T}; \qquad R = \frac{\rho a v_0}{\mu}. \tag{3}$$

In these equations ρ is the constant mass density, T is surface tension, μ is the fluid viscosity, a is the jet radius, and v_0 is the nominal velocity of the jet at the nozzle.

We wish to obtain the solution of (1), (2) on the semi-infinite jet region $z > 0$ when the *boundary conditions* at the nozzle $z = 0$ are

$$\phi(0, t) = 1, \qquad v(0, t) = 1 + \delta \cos \omega t. \tag{4}$$

A well-posed problem also requires $v_z(0, t)$ as well as a like number of downstream boundary conditions, but these are not known *a priori*. We start the computation with the *initial conditions*

$$\phi(z, 0) = 1, \qquad v(z, 0) = 1. \tag{5}$$

In order to use finite differences we lay a uniform space-time mesh on a finite length, L, of the jet. The mesh step along the jet in the z-direction will be referred to as h and the time step as k. Let i and j be the integer indexing variables along z and t, respectively; then

$$z_i = (i-1)h; \qquad t_j = (j-1)k; \qquad L = (N-1)h; \qquad L_B = (N_B - 1)h, \qquad i = 1, 2, \ldots, N, \qquad j = 1, 2, \ldots, \tag{6}$$

where z_N is the end mesh point on the jet of length L and L_B is the initially unknown length of jet from the nozzle to a breakoff point B caused by the growth of the disturbance from the nozzle (See Fig. 1).

We will adopt the notation $f_{i,j} \equiv f(z_i, t_j)$ to represent the value of the function f at the mesh point $P(i, j)$.

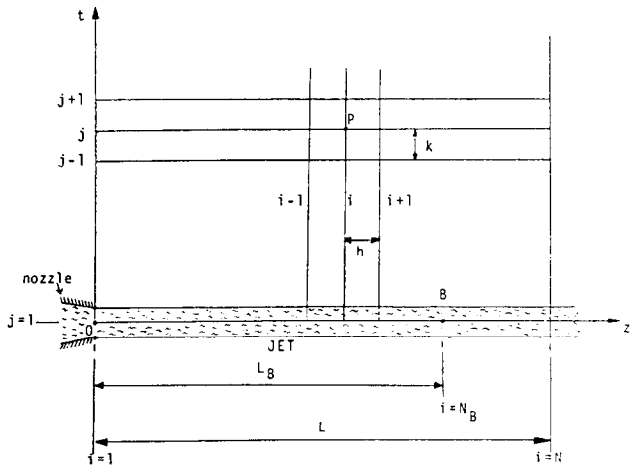

FIG. 1. Jet and space-time mesh.

3. Finite Difference (FD) Schemes

3.1. *Scheme* A. *One-Step Five-Point Spatial Averaging: Inviscid Case*

(i) FD *Formulae for Derivatives*

To avoid using the same symbol for the finite difference equations and the PDEs (1) we introduce two functions, $r(z, t)$ and $u(z, t)$, assumed to be infinitely differentiable in z and t. Later, they will be identified with ϕ and v, respectively. Then for the point $P(i, j)$ we have the following five-point central difference formulae for the space derivatives.

$$
\begin{aligned}
(r_z)_P &\equiv r'_{i,j} = \frac{1}{h}\left\{\frac{1}{12}r_{i-2,j} - \frac{2}{3}r_{i-1,j} + \frac{2}{3}r_{i+1,j} - \frac{1}{12}r_{i+2,j}\right\},\\
(r_{zz})_P &\equiv r''_{i,j} = \frac{1}{h^2}\left\{-\frac{1}{12}r_{i-2,j} + \frac{4}{3}r_{i-1,j} - \frac{5}{2}r_{i,j} + \frac{4}{3}r_{i+1,j} - \frac{1}{12}r_{i+2,j}\right\},\\
(r_{zzz})_P &\equiv r'''_{i,j} = \frac{1}{h^3}\left\{-\frac{1}{2}r_{i-2,j} + r_{i-1,j} - r_{i+1,j} + \frac{1}{2}r_{i+2,j}\right\}
\end{aligned}
\tag{7}
$$

(and similarly for u).

For the first derivatives in time we use

$$
(r_t)_P \equiv \dot{r}_{i,j} = \frac{1}{k}(r_{i,j+1} - r_{i,j})
\tag{8}
$$

(and similarly for u).

(ii) *Finite Difference Equations*

We identify r with ϕ and u with v and make the following approximations in the first of (1),

$$
\begin{aligned}
&(\phi_t)_P \approx \dot{r}_{i,j}; \qquad (\phi_z)_P \approx \tfrac{1}{2}(r'_{i,j} + r'_{i,j+1}),\\
&(v_z)_P \approx u'_{i,j}; \qquad \phi_P \approx r_{i,j}; \qquad v_P \approx u_{i,j},
\end{aligned}
\tag{9}
$$

where we have used the familar Crank–Nicolson averaging between two time levels for ϕ_z so as to obtain the corresponding implicit finite difference equation (FDE henceforth)

$$
a_{1ij}r_{i-2,j+1} + b_{1ij}r_{i-1,j+1} + c_{1ij}r_{i,j+1} + d_{1ij}r_{i+1,j+1} + e_{1ij}r_{i+2,j+1} = R_{1ij},
$$
$$
i = 3, 4, \ldots, N-2, \tag{10}
$$

where

$$a_{1ij} = A_{ij}; \qquad b_{1ij} = -8A_{ij}; \qquad c_{1ij} = 2h^3 r_{i,j}; \qquad d_{1ij} = 8A_{ij},$$
$$e_{1ij} = -A_{ij}; \qquad R_{1ij} = r_{i,j}c_{1ij} - 12hA_{ij}r'_{i,j} - kh^3 r_{i,j}u'_{i,j}, \tag{11}$$
$$A_{ij} = \frac{kh^2}{12} r_{i,j}u_{i,j}.$$

For the second of (1) we make the approximations

$$(v_t)_P \approx \dot{u}_{i,j}; \qquad (v_z)_P \approx \frac{1}{2}(u'_{i,j} + u'_{i,j+1}); \qquad (v_{zz})_P \approx \frac{1}{2}(u''_{i,j} + u''_{i,j+1}),$$

$$(v_{zzz})_P \approx \frac{1}{2}(u'''_{i,j} + u'''_{i,j+1}); \qquad (v_{zt})_P \approx \frac{1}{k}(u'_{i,j+1} - u'_{i,j}); \qquad (v_{zzt})_P \approx \frac{1}{k}(u''_{i,j+1} - u''_{i,j}),$$

$$v_P \approx u_{i,j}; \qquad (\phi_z)_P \approx r'_{i,j}; \qquad (\phi_{zz})_P \approx r''_{i,j}; \qquad (\phi_{zzz})_P \approx r'''_{i,j}; \qquad \phi_P \approx r_{i,j}, \tag{12}$$

where again we have used the Crank–Nicolson averaging for the velocity space derivatives so as to get the implicit FDE

$$a_{2ij}u_{i-2,j+1} + b_{2ij}u_{i-1,j+1} + c_{2ij}u_{i,j+1} + d_{2ij}u_{i+1,j+1} + e_{2ij}u_{i+2,j+1} = R_{2ij},$$
$$i = 3, 4, 5, \ldots, N-2, \tag{13}$$

where

$$a_{2ij} = B_{ij} - C_{ij} + D_{ij} + E_{ij} + F_{ij} + G_{ij},$$
$$b_{2ij} = -8B_{ij} + 8C_{ij} - 16D_{ij} - 8E_{ij} - 16F_{ij} - 2G_{ij},$$
$$c_{2ij} = h^6 + 30D_{ij} + 30F_{ij},$$
$$d_{2ij} = 8B_{ij} - 8C_{ij} - 16D_{ij} + 8E_{ij} - 16F_{ij} + 2G_{ij}, \tag{14}$$
$$e_{2ij} = -B_{ij} + C_{ij} + D_{ij} - E_{ij} + F_{ij} - G_{ij},$$
$$R_{2ij} = h^6 u_{i,j} - 12hB_{ij}u'_{i,j} - 12hC_{ij}u'_{i,j} + 12h^2 D_{ij}u''_{i,j}$$
$$-12hE_{ij}u'_{i,j} - 12h^2 F_{ij}u''_{i,j} + 2h^3 G_{ij}u'''_{i,j} + kh^6 X_{ij},$$

and where

$$B_{ij} = \frac{kh^5}{24} u_{i,j}; \qquad C_{ij} = \frac{h^5}{24} r_{i,j}r'_{i,j}; \qquad D_{ij} = \frac{kh^4}{48} r_{i,j}u_{i,j}r'_{i,j},$$
$$E_{ij} = \frac{kh^5}{96} r_{i,j}r'_{i,j}u'_{i,j}; \qquad F_{ij} = \frac{h^4}{96} r^2_{i,j}; \qquad G_{ij} = \frac{kh^3}{32} u_{i,j}r^2_{i,j} \tag{15}$$

and we recall that X_{ij} stands for all the surface tension terms in (2) with the derivatives taken from (7).

3.2. *Scheme* B. *One-Step Seven-Point Spatial Averaging: Inviscid Case*

(i) FD *Formulae for Derivatives*

For the point $P(i, j)$ we now use the following seven-point central difference formulae for the space derivatives:

$$(r_z)_P \equiv r'_{i,j} = \frac{1}{h}\left\{-\frac{1}{60}r_{i-3,j}+\frac{3}{20}r_{i-2,j}-\frac{3}{4}r_{i-1,j}+\frac{3}{4}r_{i+1,j}-\frac{3}{20}r_{i+2,j}+\frac{1}{60}r_{i+3,j}\right\},$$

$$(r_{zz})_P \equiv r''_{i,j} = \frac{1}{h^2}\left\{\frac{1}{90}r_{i-3,j}-\frac{3}{20}r_{i-2,j}+\frac{3}{2}r_{i-1,j}-\frac{49}{18}r_{i,j}\right.$$
$$\left.+\frac{3}{2}r_{i+1,j}-\frac{3}{20}r_{i+2,j}+\frac{1}{90}r_{i+3,j}\right\},$$

$$(r_{zzz})P \equiv r'''_{i,j} = \frac{1}{h^3}\left\{\frac{1}{8}r_{i-3,j}-r_{i-2,j}+\frac{13}{8}r_{i-1,j}-\frac{13}{8}r_{i+1,j}+r_{i+2,j}-\frac{1}{8}r_{i+3,j}\right\}$$

(and similarly for u). (16)

The first derivatives in time are given by (8).

(ii) *Finite Difference Equations*

For the first of (1) we make the same approximations as in (9) but with $r'_{i,j}$ and $u'_{i,j}$ from (16). The corresponding FDE is

$$a_{1ij}r_{i-3,j+1}+b_{1ij}r_{i-2,j+1}+c_{1ij}r_{i-1,j+1}+d_{1ij}r_{i,j+1}+e_{1ij}r_{i+1,j+1}$$
$$+f_{1ij}r_{i+2,j+1}+g_{1ij}r_{i+3,j+1}=R_{1ij}, \qquad i=4,5,6,\ldots,N-3, \tag{17}$$

where

$$a_{1ij}=-A_{ij}; \quad b_{1ij}=9A_{ij}; \quad c_{1ij}=-45A_{ij}; \quad d_{1ij}=2h^3r_{i,j},$$
$$e_{1ij}=45A_{ij}; \quad f_{1ij}=-9A_{ij}; \quad g_{1ij}=A_{ij}, \tag{18}$$
$$R_{1ij}=2h^3r_{i,j}^2-60hA_{ij}r'_{i,j}-kh^3u'_{i,j}r_{i,j}^2; \quad A_{ij}=\frac{kh^2}{60}r_{i,j}u_{i,j}.$$

For the second of (1) we use approximations (12) but with space derivatives from (16) to get the FDE

$$a_{2ij}u_{i-3,j+1}+b_{2ij}u_{i-2,j+1}+c_{2ij}u_{i-1,j+1}+d_{2ij}u_{i,j+1}+e_{2ij}u_{i+1,j+1}$$
$$+f_{2ij}u_{i+2,j+1}+g_{2ij}u_{i+3,j+1}=R_{2ij}, \qquad i=4,5,6,\ldots,N-3, \tag{19}$$

where

$$
\begin{aligned}
a_{2ij} &= -B_{ij} + C_{ij} - D_{ij} - E_{ij} - F_{ij} - G_{ij},\\
b_{2ij} &= 9B_{ij} - 9C_{ij} + \frac{27}{2}D_{ij} + 9E_{ij} + \frac{27}{2}F_{ij} + 8G_{ij},\\
c_{2ij} &= -45B_{ij} + 45C_{ij} - 135D_{ij} - 45E_{ij} - 135F_{ij} - 13G_{ij},\\
d_{2ij} &= h^6 + 245D_{ij} + 245F_{ij},\\
e_{2ij} &= 45B_{ij} - 45C_{ij} - 135D_{ij} + 45E_{ij} - 135F_{ij} + 13G_{ij},\\
f_{2ij} &= -9B_{ij} + 9C_{ij} + \frac{27}{2}D_{ij} - 9E_{ij} + \frac{27}{2}F_{ij} - 8G_{ij},\\
g_{2ij} &= B_{ij} - C_{ij} - D_{ij} + E_{ij} - F_{ij} + G_{ij},\\
R_{2ij} &= h^6 u_{i,j} - 60hB_{ij}u'_{i,j} - 60hC_{ij}u'_{i,j} + 90h^2D_{ij}u''_{i,j}\\
&\quad - 60hE_{ij}u'_{i,j} - 90h^2F_{ij}u''_{i,j} + 8h^3G_{ij}u'''_{i,j} + kh^6X_{ij},
\end{aligned}
\tag{20}
$$

and where

$$
\begin{aligned}
B_{ij} &= \frac{kh^5}{120}u_{i,j}; \qquad C_{ij} = \frac{h^5}{120}r_{i,j}r'_{i,j}; \qquad D_{ij} = \frac{kh^4}{360}r_{i,j}r'_{i,j}u_{i,j},\\
E_{ij} &= \frac{kh^5}{480}r_{i,j}r'_{i,j}u'_{i,j}; \qquad F_{ij} = \frac{h^4}{720}r^2_{i,j}; \qquad G_{ij} = \frac{kh^3}{128}u_{i,j}r^2_{i,j}
\end{aligned}
\tag{21}
$$

and we note that X_{ij} now represents all the surface tension terms (2) with the derivatives taken from (16).

3.3. *Scheme* C. *Two-Step Five-Point Spatial Averaging: Viscous Case*

(i) FD *Formulae for Derivatives*

The five-point central difference formulae for the space derivatives are exactly the same as those in (7) but with the following addition for the fourth velocity derivative.

$$
(u_{zzzz})_p \equiv u''''_{i,j} = \frac{1}{h^4}\left\{u_{i-2,j} - 4u_{i-1,j} + 6u_{i,j} - 4u_{i+1,j} + u_{i+2,j}\right\}. \tag{22}
$$

The first derivatives in time are now given by

$$(r_t)_P \equiv \dot{r}_{i,j} = \frac{1}{k}\left\{\frac{3}{2}r_{i,j} - 2r_{i,j-1} + \frac{1}{2}r_{i,j-2}\right\},$$
$$(u_t)_P \equiv \dot{u}_{i,j} = \frac{1}{2k}\{u_{i,j+1} - u_{i,j-1}\}. \tag{23}$$

(ii) FD *Equations*

In this scheme we first compute the velocity values in order to be able to compute the radius by backward differences. We now make the following approximation in the second of (1),

$$(v_z)_P \approx \frac{1}{3}(u'_{i,j-1} + u'_{i,j} + u'_{i,j+1}); \qquad (v_{zz})_P \approx \frac{1}{3}(u''_{i,j-1} + u''_{i,j} + u''_{i,j+1}),$$
$$(v_{zzz})_P \approx \frac{1}{3}(u'''_{i,j-1} + u'''_{i,j} + u'''_{i,j+1}); \qquad (v_{zzzz})_P \approx \frac{1}{3}(u''''_{i,j-1} + u''''_{i,j} + u''''_{i,j+1}),$$
$$(v_{zt})_P \approx \frac{1}{2k}(u'_{i,j+1} - u'_{i,j-1}); \qquad (v_{zzt})_P \approx \frac{1}{2k}(u''_{i,j+1} - u''_{i,j-1}), \tag{24}$$
$$(v_t)_P \approx \dot{u}_{i,j}; \qquad v_P \approx u_{i,j}; \qquad (\phi_z)_P \approx r'_{i,j}; \qquad (\phi_{zz})_P \approx r''_{i,j},$$
$$(\phi_{zzz})_P \approx r'''_{i,j}; \qquad \phi_P \approx r_{i,j},$$

where the velocity space derivatives are now averaged between three time levels. The resulting FDE is

$$a_{2ij}u_{i-2,j+1} + b_{2ij}u_{i-1,j+1} + c_{2ij}u_{i,j+1} + d_{2ij}u_{i+1,j+1} + e_{2ij}u_{i+2,j+1} = R_{2ij}, \qquad i = 3, 4, \ldots, N-2, \tag{25}$$

where

$$\begin{aligned}
a_{2ij} &= B_{ij} - C_{ij} - D_{ij} + E_{ij} - F_{ij} + G_{ij},\\
b_{2ij} &= -8B_{ij} + 16C_{ij} + 2D_{ij} - 4E_{ij} + 8F_{ij} - 16G_{ij},\\
c_{2ij} &= \tfrac{1}{2}h^6 - 30C_{ij} + 6E_{ij} + 30G_{ij},\\
d_{2ij} &= 8B_{ij} + 16C_{ij} - 2D_{ij} - 4E_{ij} - 8F_{ij} - 16G_{ij},\\
e_{2ij} &= -B_{ij} - C_{ij} + D_{ij} + E_{ij} + F_{ij} + G_{ij},\\
R_{2ij} &= \tfrac{1}{2}h^6u_{i,j-1} - 12hB_{ij}(u'_{i,j} + u'_{i,j-1}) - 12h^2C_{ij}(u''_{i,j} + u''_{i,j-1})\\
&\quad - 2h^3D_{ij}(u'''_{i,j} + u'''_{i,j-1}) - h^4E_{ij}(u''''_{i,j} + u''''_{i,j-1}) - 12hF_{ij}r'_{i,j}\\
&\quad - 12h^2G_{i,j}u''_{i,j} + kh^6X_{ij},
\end{aligned} \tag{26}$$

and where

$$
\begin{aligned}
B_{ij} &= \frac{kh^5}{36}\left\{u_{i,j} + \frac{1}{4}r'_{i,j}u'_{i,j} - \frac{6r'_{i,j}}{Rr_{i,j}}\right\},\\
C_{ij} &= \frac{kh^4}{36}\left\{\frac{3r'^2_{i,j}}{2R} + \frac{r_{i,j}r''_{i,j}}{2R} - \frac{3}{R} - \frac{r_{i,j}r'_{i,j}}{2}u_{i,j}\right\},\\
D_{ij} &= \frac{kh^3}{6}\left\{\frac{r_{i,j}r'_{i,j}}{R} - \frac{r^2_{i,j}}{8}u_{i,j}\right\},\\
E_{ij} &= \frac{kh^2r^2_{i,j}}{24R}, \quad F_{ij} = \frac{h^5}{48}r_{i,j}r'_{i,j}, \quad G_{ij} = \frac{h^4}{192}r^2_{i,j},
\end{aligned}
\tag{27}
$$

and again we recall that X_{ij} represents all the surface tension terms with the radius space derivatives given by (17).

Next we make the following approximation in the first of (1),

$$
(\phi_t)_p \approx \dot{r}_{i,j}; \qquad (\phi_z)_p \approx r'_{i,j}; \qquad \phi_p \approx r_{i,j}; \qquad (v_z)_p \approx u'_{i,j}; \qquad v_p \approx u_{i,j} \tag{28}
$$

with $r'_{i,j}$ and $u'_{i,j}$ from (7) and $\dot{r}_{i,j}$ from (23) to get the implicit FDE

$$
a_{1ij}r_{i-2,j} + b_{1ij}r_{i-1,j} + c_{1ij}r_{i,j} + d_{1ij}r_{i+1,j} + e_{1ij}r_{i+2,j} = R_{1ij}, \qquad i = 3, 4, \ldots, N-2, \tag{29}
$$

where

$$
\begin{aligned}
a_{1ij} &= A_{ij}; \qquad b_{1ij} = 8A_{ij}; \qquad C_{1ij} = 3h^3 + kh^3u'_{i,j},\\
e_{1ij} &= -A_{ij}; \qquad R_{1ij} = h^3(4r_{i,j-1} - r_{i,j-2}); \qquad A_{ij} = \frac{kh^2}{6}u_{i,j}.
\end{aligned}
\tag{30}
$$

4. Implementation of the FD Schemes

(i) *Preamble*

The computational effort in this problem can be quite large even on machines such as the CDC 7600. Because of the nonlinearity of the equations the matrix coefficients for the schemes have to be computed at every point on the space-time lattice and this consumes most of the computing time. Therefore the computation of these coefficients needs to be as efficient as possible. In order to keep an accurate record of the number

of cycles of the input periodic excitation at the nozzle we found it convenient to divide one cylce into exactly p partitions and compute the time step by

$$k = 2\pi/\omega p. \tag{31}$$

A good resolution of a cycle requires $p > 12$. With k so computed we know that after np ($n = 1, 2,...$) time steps exactly n cycles of the input excitation will have gone downstream from the nozzle. As the breakoff point is approached we can examine the solution and then advance it by, say, half a cycle. This is particularly useful in studying the details of drop formation a few cycles before the jet breaks.

It is well known in numerical analysis that some schemes in FD methods require more boundary and/or initial conditions than are prescribed for the problem to be solved. When confronted with this situation one has to estimate the additional conditions by some means as discussed by Ilan [10] and Gottlieb and Turkel [11]. In this problem the presence of high space derivatives in the second of (1) necessitates estimation of additional nozzle conditions and the two-step scheme requires more initial conditions to implement. The details of how this was accomplished are given below for the three schemes.

It is relevant at this point to mention that no stability criterion was obtained analytically for any of the schemes. Usually for linear PDEs one can quickly establish a relation between k and h under which a scheme is stable. A few researchers have carried out theoretical stability analyses for nonlinear equations. Hirt [17] describes a stability analysis based on the examination of truncation errors which is applicable to both linear and nonlinear equations. However, such analyses can be applied only to relatively simple nonlinear equations. Many researchers have abandoned the analytical approach and instead concentrate on numerical experiments for establishing the stability conditions for nonlinear problems. For example, Miller [18] describes an experimental method based on parallel calculations for initial value problems in which two sets of initial conditions differing by a small perturbation parameter are used and the resulting solutions are continuously monitored. For time dependent (and reversible) problems Miller [18] also suggests running the scheme first forward in time from the initial conditions and then backward in time to the initial conditions. In this work conditions for stability were established by numerical experimentation. More will be said about this later.

(ii) *Scheme* A

From the FDE (13) it can be seen that values of u must be known at two grid points on both ends of the jet for all time. One of them, at the nozzle, is the given velocity boundary condition in the second of (4), the other one must be estimated. Since we are using five points to average the derivatives it is reasonable to assume that, for small h,

$$u_{2,j} = u_{1,j}, \qquad j = 2, 3, 4,..., \tag{32}$$

where $u_{1,j}$ is obtained from the boundary condition (4). To ease our conscience we make the following correction at every time step,

$$\tilde{u}_{2,j} = \tfrac{1}{2}(u_{1,j} + u_{3,j}), \tag{33}$$

where $u_{3,j}$ is computed implicitly by a pentadiagonal matrix system using the values of r and u at the previous time step and the end conditions.

Far downstream we can safely assume that

$$u_{N,j} = u_{N-1,j} = 1, \qquad j = 2, 3,..., \tag{34}$$

where the length, $L = (N = 1)h$, of the jet we start with is considerably longer than the length, $L_B = (N_B - 1)h$, of the jet from the nozzle to the expected breakoff point. The first of (1) has only first space derivatives and therefore one should seek a scheme which needs only one condition at each end. Unfortunately, the tridiagonal schemes or explicit schemes that would satisfy this criterion are among the schemes unsuitable for this problem. Several such schemes were tried, and most were found to be unsuitable because of numerical instabilities or instabilities caused by the solution itself as the disturbance propogated downstream. In some cases the scheme appeared to be stable but gave an incorrect solution. These unsuitable schemes are discussed in Shine [20]. The pentadiagonal FDE (10) is the lowest-order scheme which gave meaningful results. Having made assumption (32) on the velocity we can make a similar assumption on the radius, since they are related by the continuity equation. Therefore we assume

$$r_{2,j} = r_{1,j}, \qquad j = 2, 3,..., \tag{35}$$

where $r_{1,j}$ is set equal to the first boundary condition (4), followed again by the correction

$$\tilde{r}_{2,j} = \tfrac{1}{2}(r_{1,j} + r_{3,j}). \tag{36}$$

Far downstream, where the jet is still undisturbed, we again set

$$r_{N,j} = r_{N-1,j} = 1, \qquad j = 2, 3, 4,.... \tag{37}$$

We remark here that for fast jets (high Weber numbers) and small perturbation amplitude δ, at the nozzle, assumptions (32) and (35) are expected to be good since the jet is observed experimentally to come off the nozzle with almost zero slope (i.e., $\phi_z(0, t) = 0$) so that the continuity equation also gives $v_z(0, t) = 0$. Good results are obtained in these case even without the associated corrections (33) and (36).

The given initial conditions (5) are sufficient to get a joint scheme started. Therefore by setting $j = 1$ in (10) and using the first of (4) together with (35) and (37) we can compute all the values of r_i ($i = 3, 4,..., N - 2$) at $j = 2$ by solving the resulting pentadiagonal matrix equation. The classical fast recursion method for solving such an equation was used; see Conte and Dames [9] and Shine [20]. Then

(13) is used to compute all the $u_{i,2}$ by again solving a pentadiagonal system and making use of the end conditions (32) and (34). We then increment j by one and return to (10), then return again to (13) and increment j. Shuttling between the two equations at every time step we can advance the solution simultaneously by solving the two pentadiagonal systems (10) and (13) from the initial conditions, subject to the end conditions, which we pick at every time step as we march forward in time. The solution is advanced in time until the disturbance, which moves downstream growing in amplitude, causes the radius to become just less than zero at a point downstream or until the velocity exceeds a chosen absolute maximum value, whichever comes first. We throw away these last values of r and u and take the previous values as our approximate FD solution for ϕ and v for a disturbance growing from the nozzle to the breakoff point.

(iii) *Scheme* B

It is clear from (17) and (19) that we need two additional conditions for r and u at the nozzle to implement this scheme, which has higher spatial accuracy than Scheme A. The perturbation solution in Bogy [2] was used for obtaining the additional conditions. This approach gives

$$\begin{aligned} v_z(0,t) &= \delta A_1 \sin \omega t; \qquad v_{zz}(0,t) = -\delta A_2 \cos \omega t, \\ \phi_z(0,t) &= \delta A_3 \sin \omega t; \qquad \phi_{zz}(0,t) = -\delta A_4 \cos \omega t, \end{aligned} \tag{38}$$

where

$$\begin{aligned} &A_1 = 0.524871528; \qquad A_2 = 0.275103636, \\ &A_3 = -0.262435764; \qquad A_4 = -0.275330604, \\ &\text{for} \quad \omega = 0.525; \qquad W = 250. \end{aligned} \tag{39}$$

By use of first order forward FD approximations to the derivatives in (38) we can estimate the additional conditions as

$$\begin{aligned} u_{2,j} &= u_{1,j} + h\,\delta A_1 \sin\{\omega(j-1)k\}, \\ u_{3,j} &= 2u_{2,j} - u_{1,j} - h^2\,\delta A_2 \cos\{\omega(j-1)k\}, \\ r_{2,j} &= 1 + h\,\delta A_3 \sin\{\omega(j-1)k\}, \\ r_{3,j} &= r_{2,j} - 1 - h^2\,\delta A_4 \cos\{\omega(j-1)k\}, \\ j &= 1, 2, 3, \ldots. \end{aligned} \tag{40}$$

Far downstream, where the jet is still undisturbed, we again set

$$\begin{aligned} u_{N,j} &= u_{N-1,j} = u_{N-2,j} = 1.0, \\ r_{N,j} &= r_{N-1,j} = r_{N-2,j} = 1.0. \end{aligned} \tag{41}$$

The given initial conditions are enough to get this scheme started. The solution is obtained by shuttling between (17) and (19) at every time step as described above by solving the heptadiagonal matrix systems. The recursion method was extended to do that in Shine [20].

(iv) *Scheme* C

The additional end conditions on r and u required for this scheme are the same as those for Scheme A. However, we also need two additional initial conditions. Since we start with an undisturbed jet at $t = 0$ it follows that

$$\begin{aligned} \phi_z(z, 0) = \phi_{zz}(z, 0) = \phi_{zzz}(z, 0) = 0, \\ v_z(z, 0) = v_{zz}(z, 0) = v_{zzz}(z, 0) = v_{zzzz}(z, 0) = 0, \end{aligned} \tag{42}$$

from which the first of (1) gives

$$\phi_t(z, 0) = 0 \tag{43}$$

so that

$$r_{i,2} = r_{i,1} = 1, \qquad i = 1, 2, ..., N, \tag{44}$$

where $r_{i,1}$ is determined from the initial condition in the first of (4). Also (42) in the second of (1) gives

$$v_t(z, 0) - \tfrac{1}{8} v_{zzt}(z, 0) = 0. \tag{45}$$

Using the approximations in the second of (8) and the sixth of (12) with $u''_{i,j}$ taken from (7) we can solve (45) for $u_{i,2}$.

Thus with two starting rows for u and r this scheme can be implemented. Here, however, we start with the FDE (25) and shuttle between it and (29) at every time step by solving pentadiagonal matrix equations.

5. Numerical Results and Discussions

5.1. *Stability*

As mentioned earlier the mesh size for stability was determined by numerical experimentation. We arbitrarily chose a small value of h (the largest is of course determined by the frequency, ω, of the excitation at the nozzle) and then ran the schemes for only a few time steps for various values of k (the largest value of which is also determined by ω). The computed values of r and u near the nozzle were studied and compared with the nozzle conditions. If there was a significant difference it was a sure sign that large numerical instabilities would quickly develop at the nozzle before we could complete even one cycle of the input excitation. This was confirmed for some of the cases by running the scheme for a longer time. For

example, Scheme B develops instabilities similar to Fig. 2 for very small values of h, say, 0.05, regardless of the value of k, when the old values of r are used in computing the velocity values, but it is always stable when the latest values of r computed by the first of (1) are used in the computation of the velocity values.

It was therefore possible to quickly predict when nozzle instabilities would occur by this trial and error method. However, numerical instabilities that are induced by the solution itself cannot be so easily predicted; the scheme has to be run until such instabilities develop as the disturbance moves downstream. For example, Fig. 3 shows a case in which numerical instabilities develop after 6 cycles of apparently good solution; for the conditions shown the wave is supposed to grow for about 11 cycles before it breaks the jet at $z \simeq 130$ as shown in Fig. 7a.

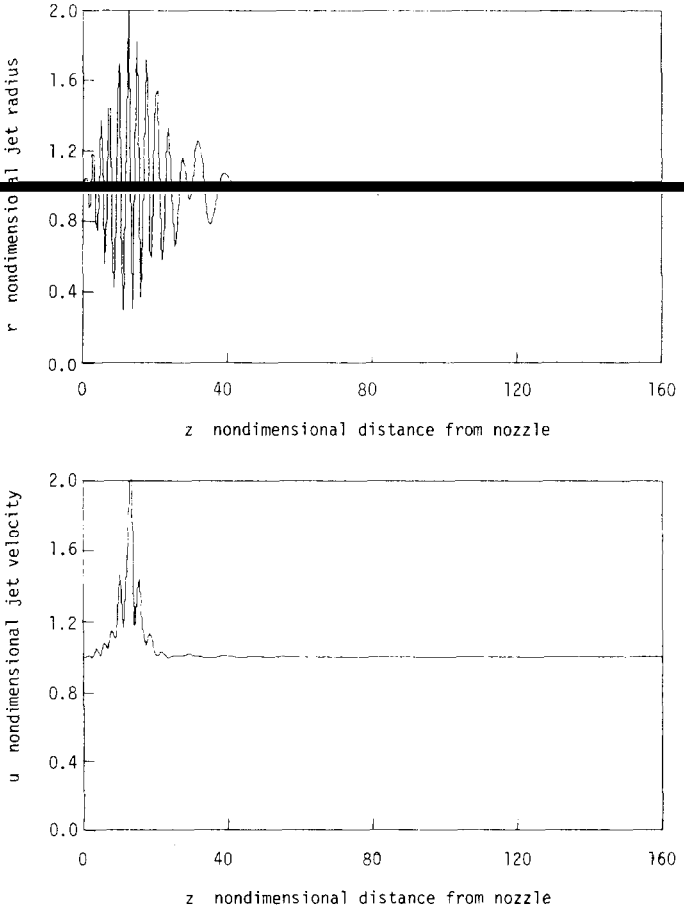

FIG. 2. Radius and velocity Profiles. $\delta = 0.01$, $\omega = 0.525$, $W = 250$, $p = 100$ ($k \approx 0.12$), $h = 0.5$; typical instabilities at nozzle.

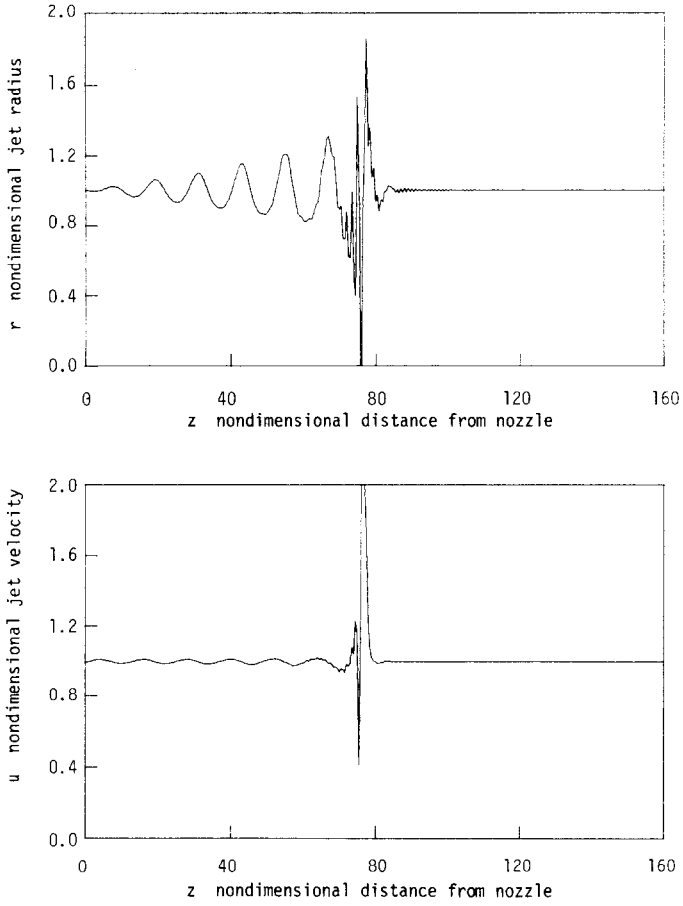

FIG. 3. Radius and velocity profiles. $\delta = 0.01$, $\omega = 0.525$, $W = 250$, $p = 100$ ($k \approx 0.12$), $h = 0.5$, $t = 6.33$ input cycles. Numerical instabilities caused by solution.

As the disturbance moves and grows downstream the jet remains undisturbed ahead of it. This was a very helpful observation because it enabled us to cut the computing time by a factor of about 2 by making use of the fact that after exactly p time steps one cycle of the excitation at the nozzle has gone downstream. So at $t = 0$ we start with an undisturbed length of jet of about two wave lengths and after exactly p steps we increment the length by a value slightly longer than the wave length, and compute for p steps and then increment the length again and so on. In this fashion the solution is computed using a staggered length. Of course with this technique we have to know roughly where jet breakoff is going to occur. This was estimated by computing with the largest mesh size possible or from the results of the perturbation solutions of these equations in Bogy [2, 3].

5.2. *Effect of Mesh Size*

For reasonable resolution of the periodic disturbance the frequency determines the coarsest possible space-time grid. With a coarse mesh a very rough solution of the problem is obtained in which only the main drops are shown to form and a breakoff point too near the nozzle is predicted. This is shown in Fig. 4, where $z_B \simeq 110$ instead of the correct value of $z_B = 130$ for the conditions indicated. The accurate breakoff point can be calculated from results given in Bogy [4], known to agree with experiment. It is also related to the number of time steps by

$$z_B = \frac{2\pi t_B}{\omega}, \tag{46}$$

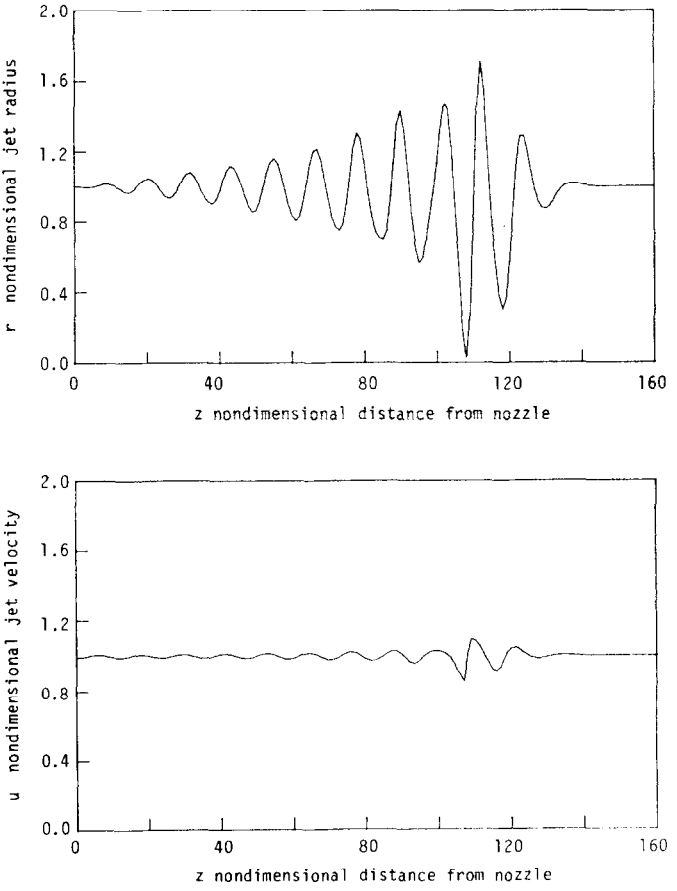

FIG. 4. Scheme A: Radius and velocity profiles just before jet breakup. $\delta = 0.01$, $\omega = 0.525$, $W = 250$, $p = 12$ ($k \approx 1.0$), $h = 1.0$, $t_B = 11.5$ input cycles.

where t_B is the time to breakoff, measured in number of cycles of the input nozzle excitation. If the accuracy is insufficient due to the coarseness of the mesh for the scheme used then z_B shown in the computed radius profiles differs significantly from what it should be according to (46). This seems to be an inherent difficulty with simultaneous FD solution of more than one time-dependent equations. The space-time mesh has to be made very small to minimize the lag or lead of the values computed by one of the equations over those computed by the other equations. A good check on the mesh size is the calculation of a breakoff point that agrees with (46).

As the mesh is refined we, expectedly, get better and better solutions, the breakoff point converges to the correct value, and small satellite drops begin to form between the main drops as the breakoff point is approached. Also less distortion (due to v and the derivatives of ϕ and v becoming very large) of the leading cycle occurs as it

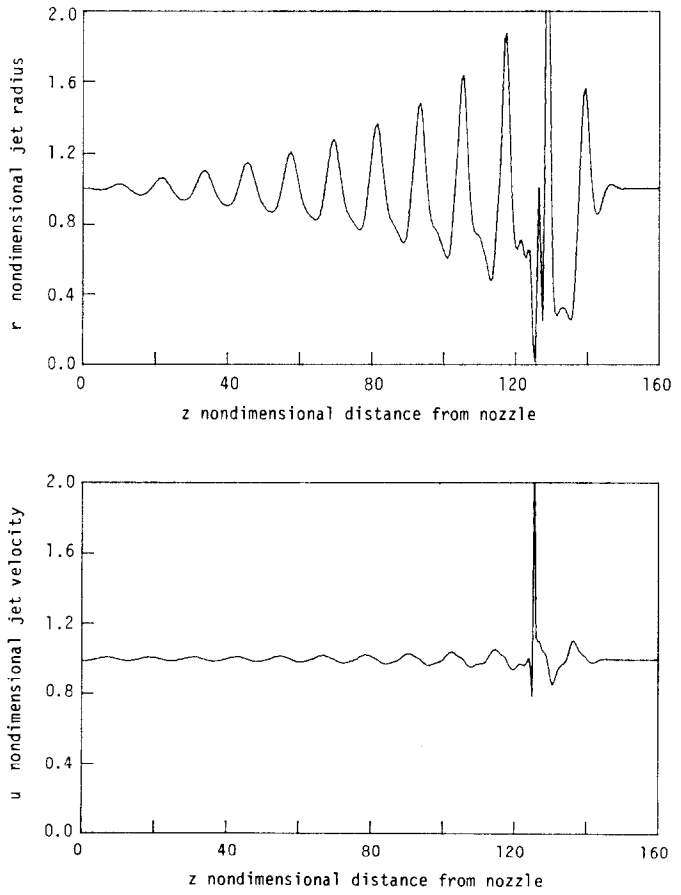

FIG. 5. Scheme A: Radius and velocity profiles just before jet breakup. $\delta = 0.01$, $\omega = 0.525$, $W = 250$, $p = 100$ ($k \approx 0.12$), $h = 0.5$, $t_B = 11.49$ input cycles.

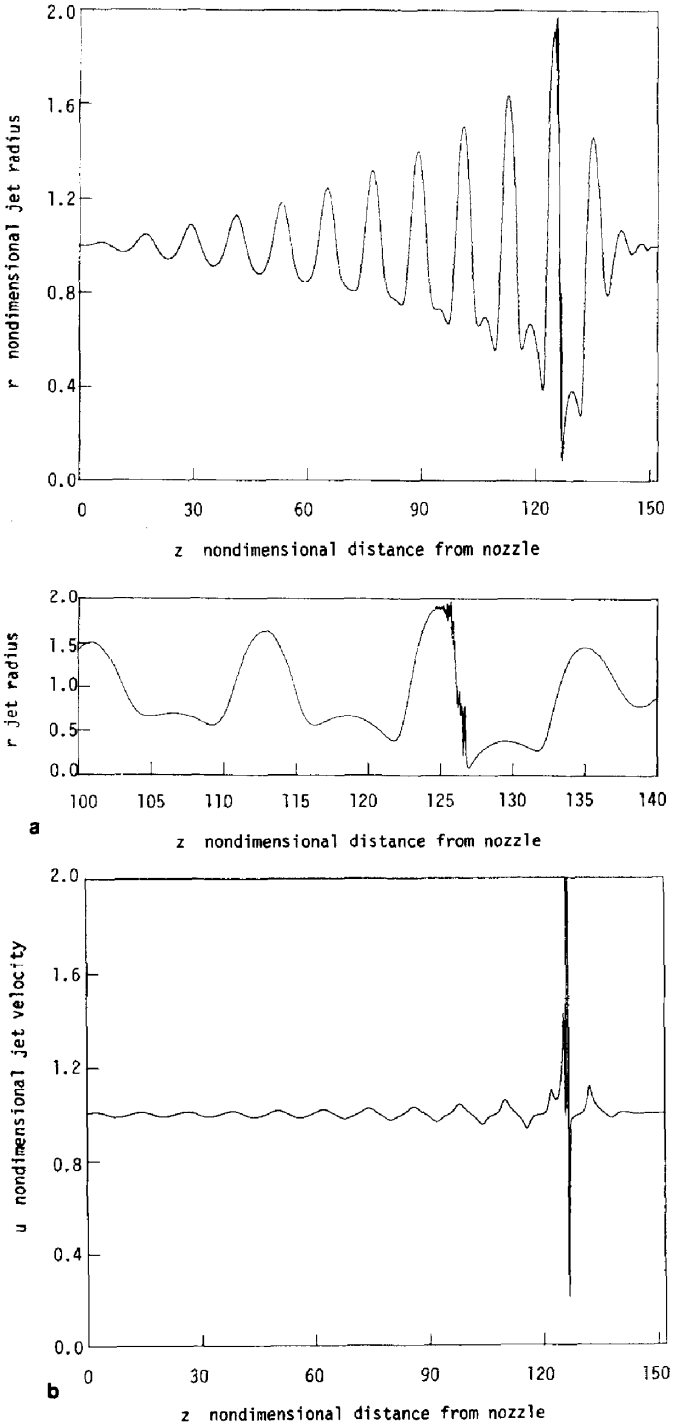

FIG. 6. Scheme A: (a) Radius profile just before jet breakup. $\delta = 0.01$, $\omega = 0.525$, $W = 250$, $p = 200$ ($k \approx 0.06$), $h = 0.05$, $t_B = 11.15$ input cycles. (b) Velocity profile for previous radius profile.

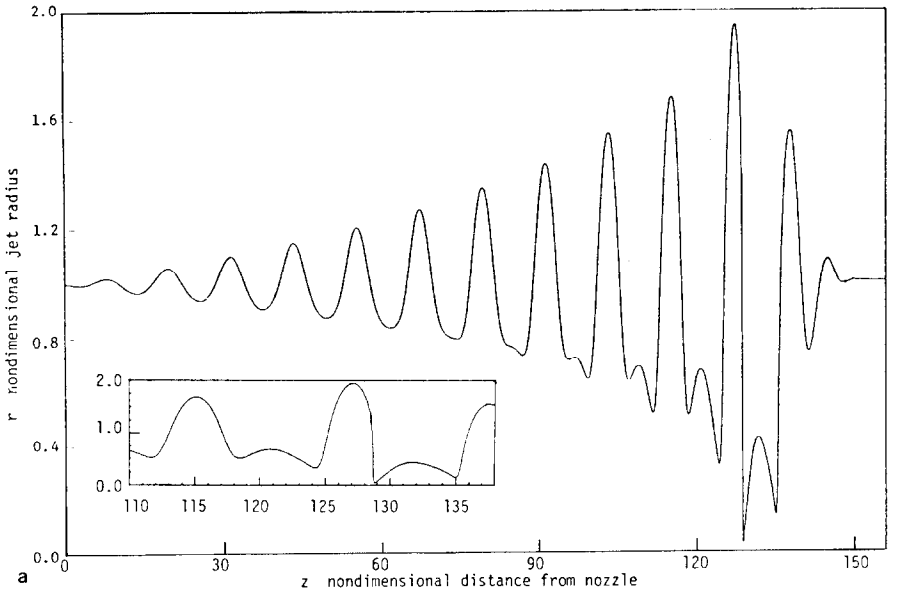

FIG. 7. Scheme B: (a) Radius profile just before jet breakup. $\delta = 0.01$, $\omega = 0.525$, $W = 250$, $p = 200$ ($k \approx 0.06$), $h = 0.05$, $t_B = 11.37$ input cycles. (b) Velocity profile for previous radius profile. (c) Comparison of results from Scheme B with the perturbation solution in Ref. [3].

reaches breakoff. And of course as we refine the mesh for the same length of jet the computing times increases.

Scheme A. Figures 4, 5, and 6 show the results of this scheme with the mesh progressively refined. It is clear that the accuracy of this scheme is not good enough, even with the finest mesh used, to predict the correct breakoff point or give a smooth solution for the leading cycle near breakoff. The joint accuracy of the scheme is shown in Shine [20] to be $O(k, h^2)$ and this is not good enough to handle the large derivatives that occur near breakoff. Even at $h = 0.05$ and $k \approx 0.06$ breakoff is shown in Fig. 6 to be at $z_B = 127$ instead of $z_B = 130$ for the conditions indicated, and the leading cycle is still noticeably distorted.

Scheme B. This scheme is shown in Shine [20] to be $O(k, h^4)$ accurate and Fig. 7 shows the results at $h = 0.05$ and $k \approx 0.06$. The breakoff point $z_B = 129$ shown is very close to the correct value of 130. Also a smooth solution for the leading cycle at breakoff is obtained.

Scheme C. The previous two schemes are inviscid and at breakoff they tend to predict very large velocity values and sometimes even negative values. It is for this reason that we investigated inviscid flows by this viscous scheme. Since it is second-order accurate in time the breakoff point is predicted reliably for reasonably fine

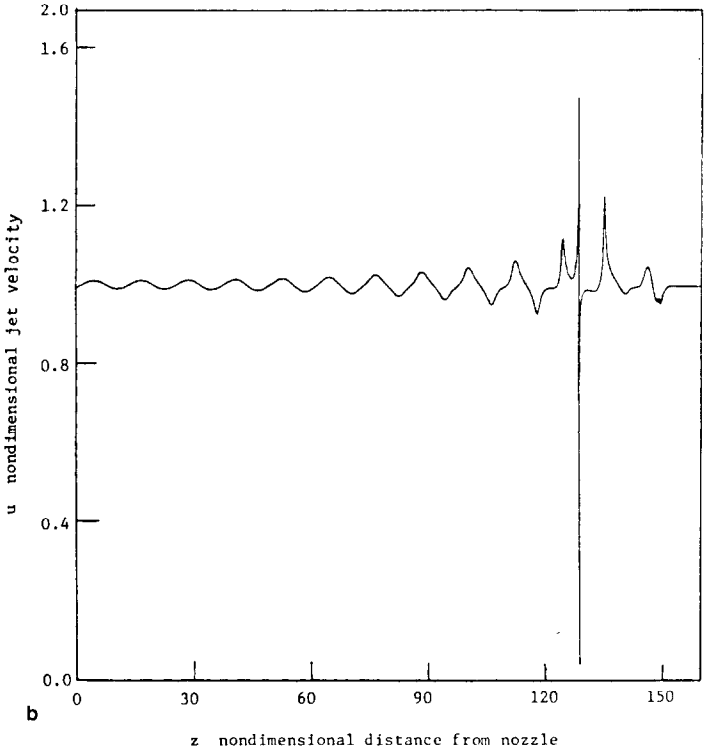

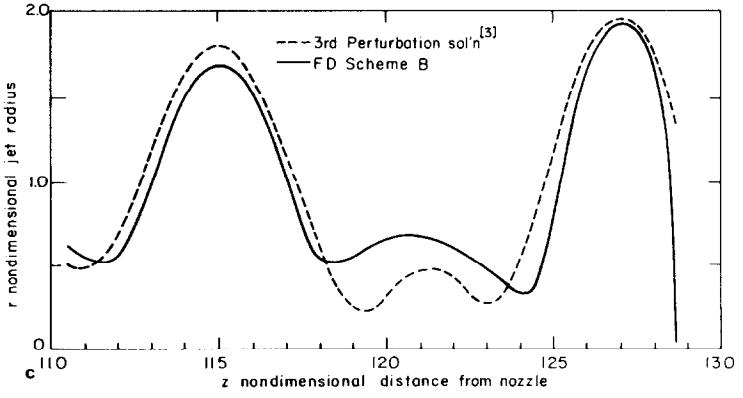

FIG. 7—*Continued.*

mesh. Also with this scheme we studied the effect of viscosity on the growth of the disturbance as in Fig. 15.

5.3. *General Results for the Problem*

(i) *Effect of Frequency*

The frequency, ω, of the periodic excitation at the nozzle has an interesting effect on the propagation of the disturbance from the nozzle in that if $\omega > 1$ the generated wave is stable and therefore does not grow in amplitude, to break the jet, as illustrated in Figs. 8 and 9. However, if $\omega < 1$ the resulting wave grows in amplitude until it finally breaks the jet at a definite point downstream, as shown in Fig. 7a. For the same unstable $\omega < 1$, the breakoff point will depend on other parameters as

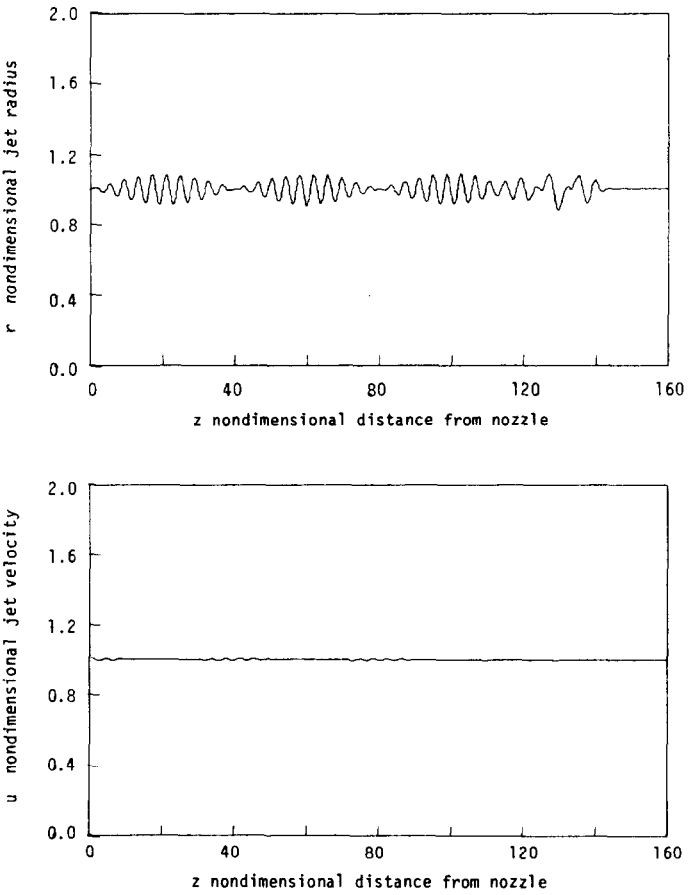

FIG. 8. Scheme A: Radius and velocity profiles. $\delta = 0.01$, $\omega = 1.6$, $W = 250$, $p = 32$ ($k \approx 0.12$), $h = 0.125$, $t = 33$ input cycles.

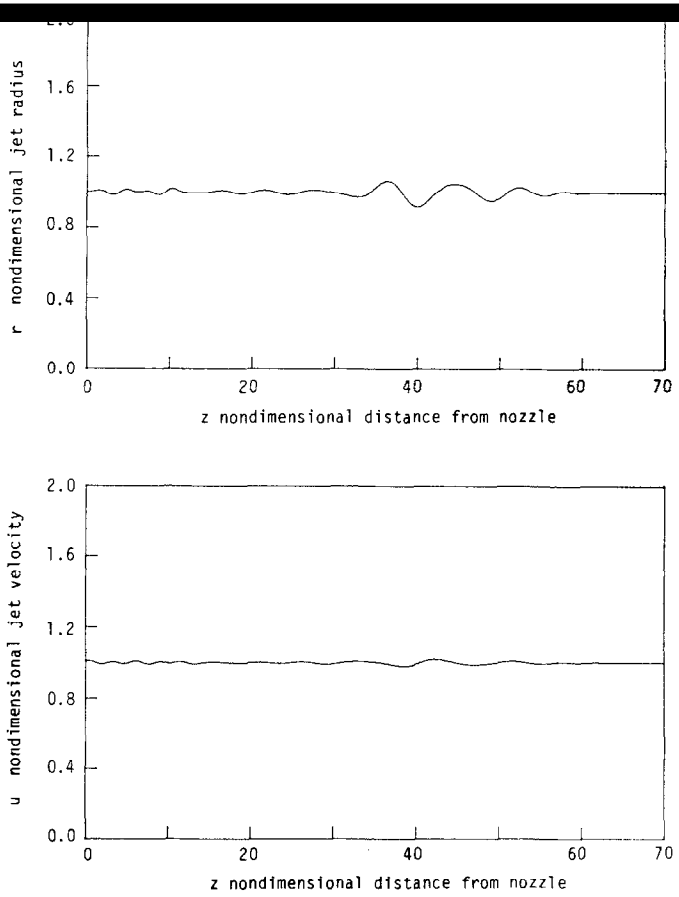

FIG. 9. Scheme A: Radius and velocity profiles. $\delta = 0.01$, $\omega = 1.4$, $W = 9$, $p = 50$ $(k \approx 0.09)$, $h = 0.1$, $t = 9$ input cycles.

discussed below. This effect of frequency on the wave propagation agrees with that obtained by perturbation analysis of the same equations by Bogy [4].

(ii) *Drop Formation*

For the unstable frequencies the jet breaks up into main drops whose diameter is about twice that of the nozzle, as shown in Figs. 10–13. Formation of smaller drops, referred to in the literature as satellite drops, interspersed between the main drops is predicted for the fast jets when the space-time lattice is fine enough to resolve that behavior, as shown in Figs. 7, 11, 12 and 13. Again, similar results were also obtained from the Cosserat equations by Bogy [2, 3] using perturbation techniques to solve the equations.

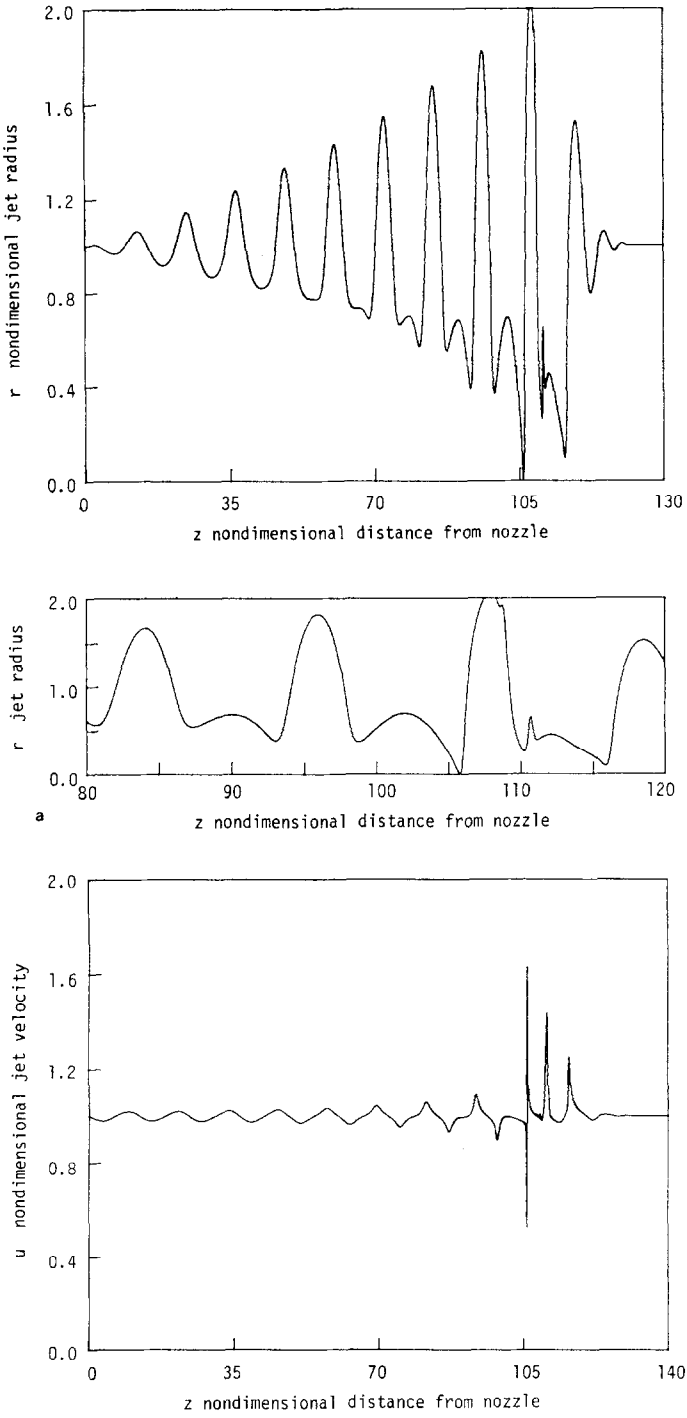

FIG. 10. Scheme C: (a) Radius profile just before jet breakup. $\delta = 0.02$, $\omega = 0.525$, $W = 250$, $R = 500$, $p = 240$ ($k \approx 0.05$), $h = 0.05$, $t_B = 9.75$ input cycles. (b) Velocity profile for previous radius profile.

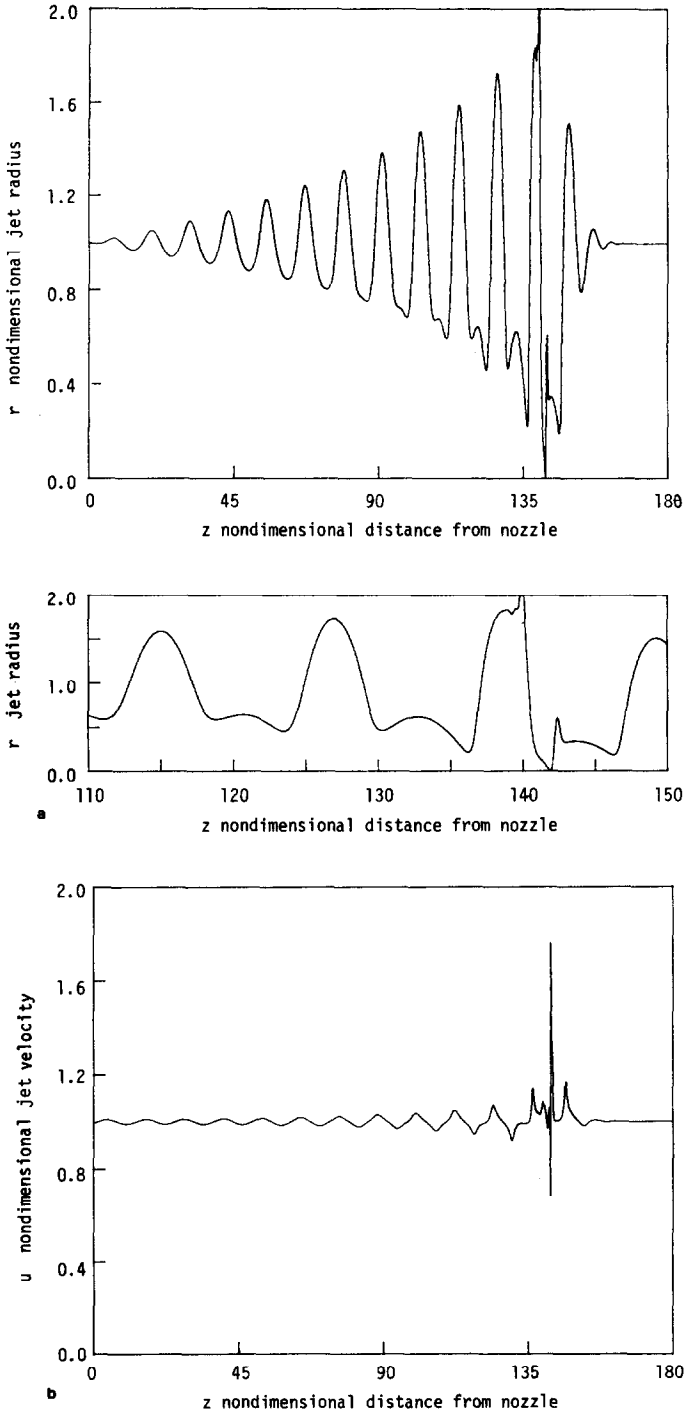

FIG. 11. Scheme C: (a) Radius profile just before jet breakup. $\delta = 0.01$, $\omega = 0.525$, $W = 250$, $R = 500$, $p = 240$ ($k \approx 0.05$), $h = 0.05$, $t_B = 12.33$ input cycles. (b) Velocity profile for previous radius profile.

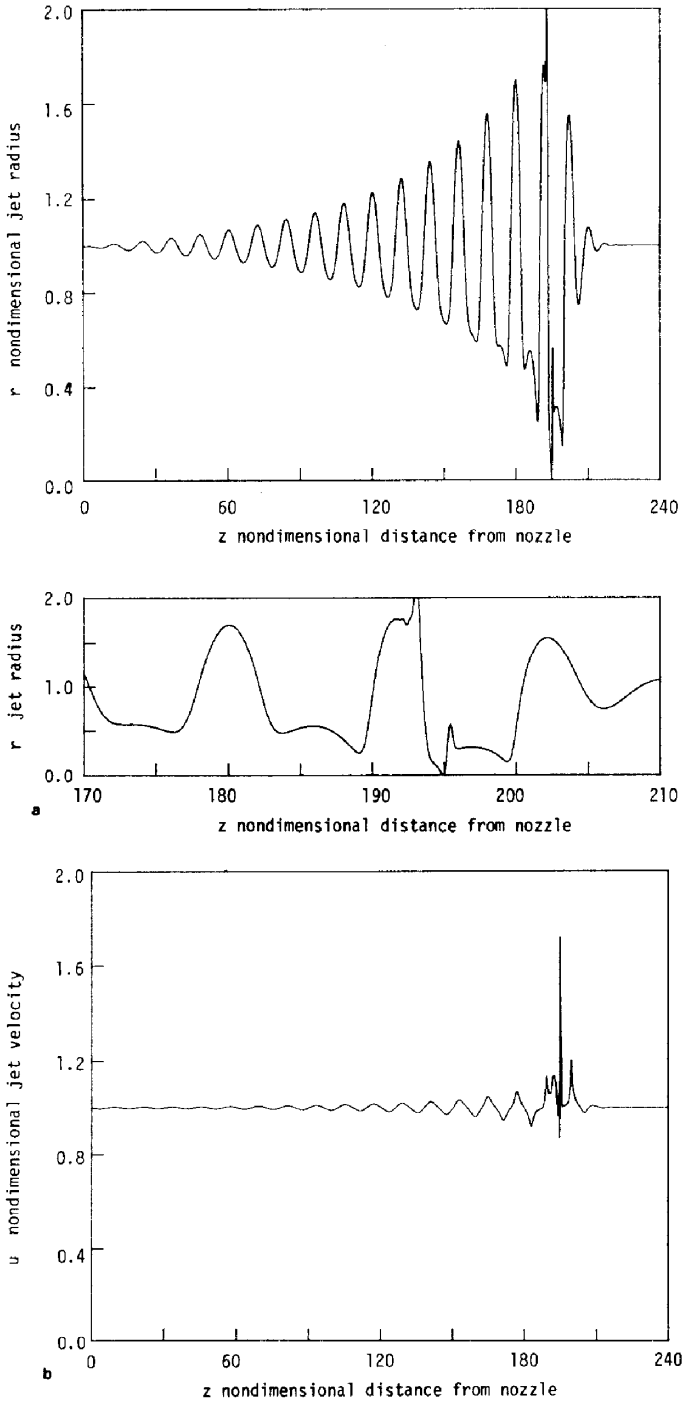

FIG. 12. Scheme C: (a) Radius profile just before jet breakup. $\delta = 0.0035$, $\omega = 0.525$, $W = 250$, $R = 500$, $p = 240$ ($k \approx 0.05$), $h = 0.05$, $t_B = 16.77$ input cycles. (b) Velocity profile for previous radius profile.

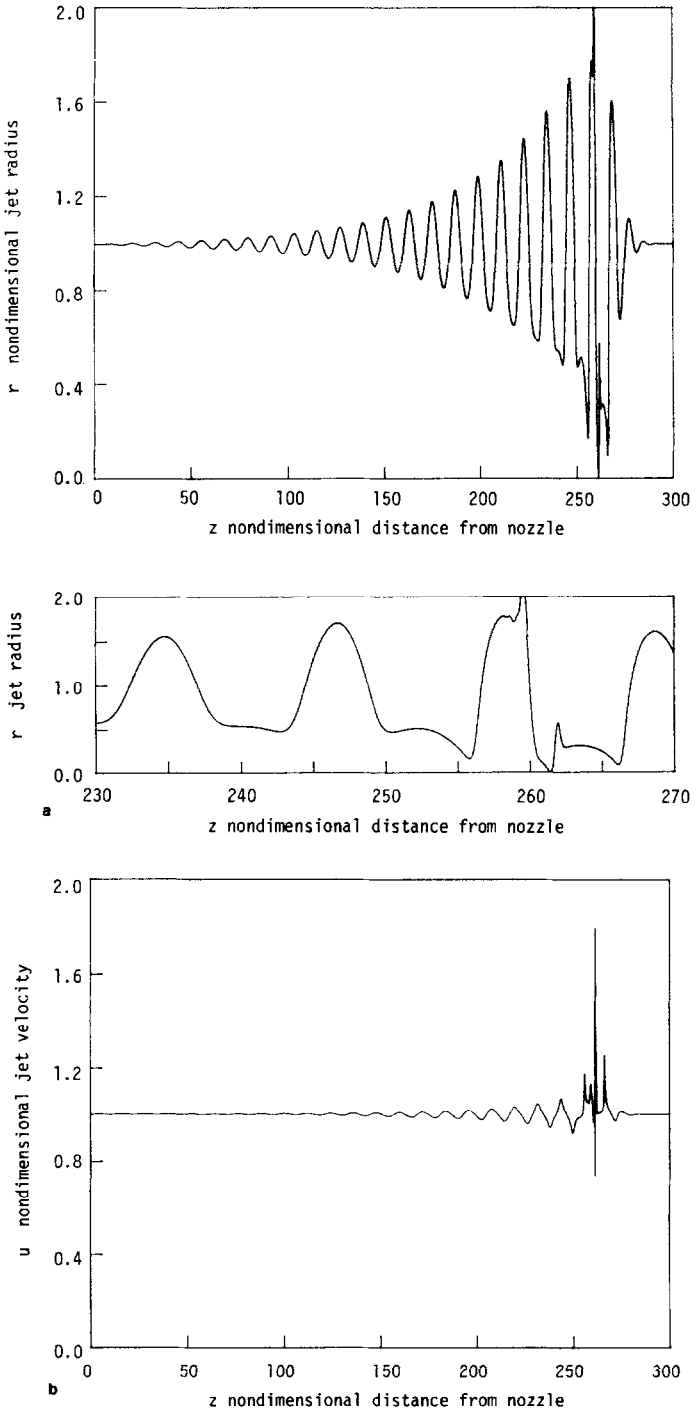

FIG. 13. Scheme C: (a) Radius profile just before jet breakup. $\delta = 0.001$, $\omega = 0.525$, $W = 250$, $R = 500$, $p = 240$ ($k \approx 0.05$), $h = 0.05$, $t_B = 22.33$ input cycles. (b) Velocity profile for previous radius profile.

(iii) *Effect of Amplitude of Excitation*

As the amplitude, δ, of the velocity perturbation at the nozzle is reduced the jet breaks farther from the nozzle, as shown in Figs. 10–13. Also the amplitude of the disturbance is known to affect the behaviour of the satellite drops. For very small δ they are rear merging whereas for larger δ they are forward merging as calculated by the third perturbation solution of Bogy [3] and demonstrated experimentally by Pimbley and Lee [8]. However, for the schemes presented here and the finest space-time grid we used this behaviour of the satellite drops was not predicted. This is possibly because the results at the downstream and of the leading cycle at breakoff are not very reliable. This is a singular point where the derivatives of ϕ and v, and v itself, are very large. For a numerically reliable prediction we should obtain the correct behaviour of these drops one cycle before breakoff point. A considerable effort was put into trying to achieve this but we were limited by computing time and

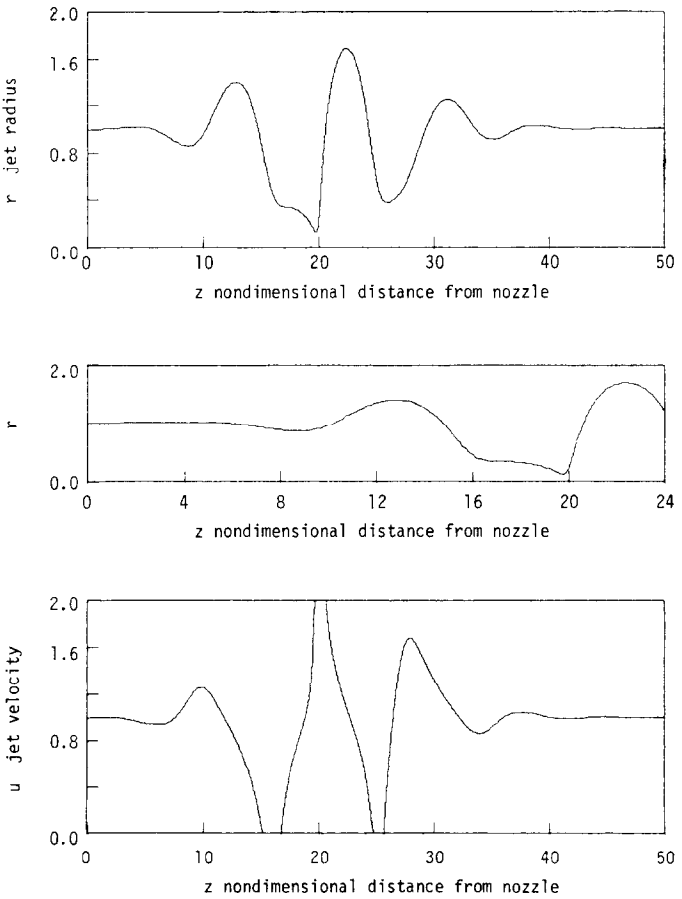

FIG. 14. Scheme B: Radius and velocity profiles just before jet breakup. $\delta = 0.01$, $\omega = 0.525$, $W = 1$, $p = 240$ ($k \approx 0.05$), $h = 0.1$, $t_B = 1.75$ cycles.

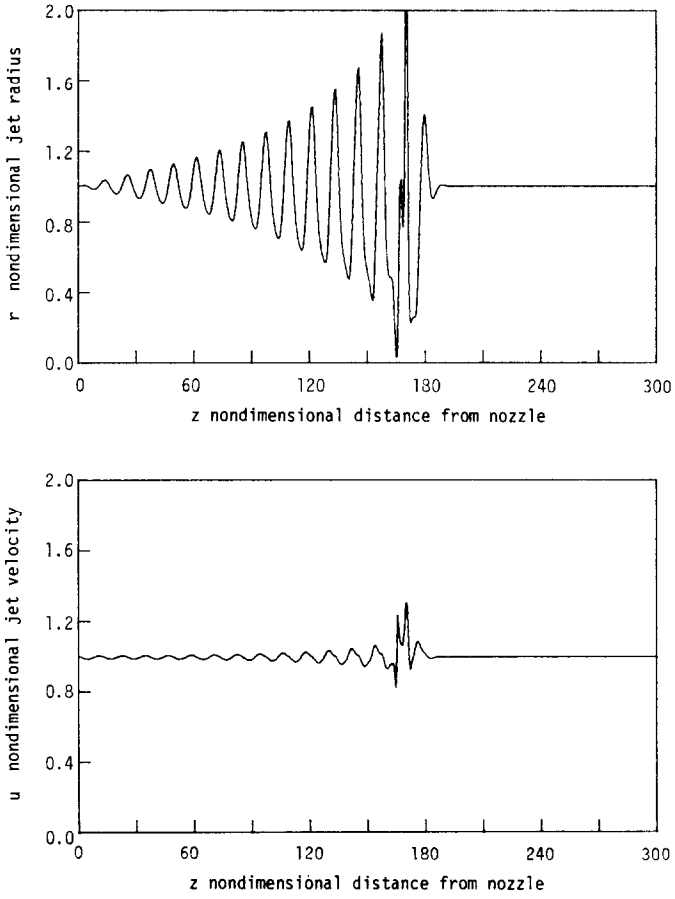

FIG. 15(a). Scheme C: Radius and velocity profiles just before jet breakup. $\delta = 0.01$, $\omega = 0.525$, $W = 250$, $R = 100.0$, $p = 100$ ($k \approx 0.12$), $h = 0.5$, $t_B = 15.84$ input cycles.

cost. The finest mesh used was $h = 0.05$, $k = 0.05$ with two time refinements to $k \approx 0.025$ and $k \approx 0.0125$ for the last two cycles. The result with Scheme B is the same as in Fig. 7 and with Scheme C the same as in Fig. 11. No value of h smaller than 0.05 was used because then the computing time would be prohibitive.

Fig. 7c shows a comparison over the last cycle before breakoff of the results obtained by Scheme B with those obtained by the third perturbation solution in Bogy [3]. The difference between the two solutions is less nearer the nozzle. It is possible that this difference is merely due to the fact that different problems were solved in the two instances. The FD solution was for an initial-boundary value problem in which the initial jet was of uniform flow. The perturbation solution was for a steady time harmonic problem, i.e., without initial conditions and transients.

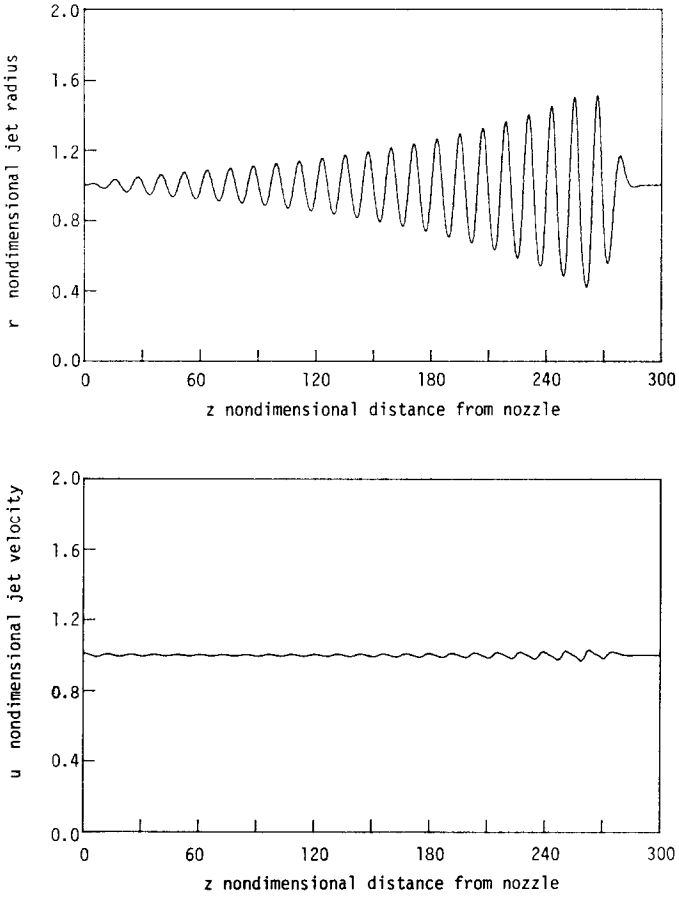

FIG. 15(b). Scheme C: Radius and velocity profiles. $\delta = 0.01$, $\omega = 0.525$, $W = 250$, $R = 25.0$, $p = 100$ ($k \approx 0.12$), $h = 0.5$, $t = 23$ input cycles.

(iv) *Effect of Jet Velocity*

As we decrease the Weber number (or the velocity at the nozzle) the jet breakoff point occurs nearer the nozzle. This is illustrated by Figs. 7 and 14. This also agrees with the perturbation solution of Bogy [4].

(v) *Effect of Viscosity*

Viscosity appreciably affects the breakoff point of the jet, as illustrated in Figs. 11 and 15a–c. It is evident that, other parameters being kept the same, the growth of the disturbance from the nozzle is considerably slowed as R decreases (i.e., as the fluid becomes more viscous) until a point is reached where the higher viscosity can dampen the growth of the disturbance and therefore practically no jet breakup occurs.

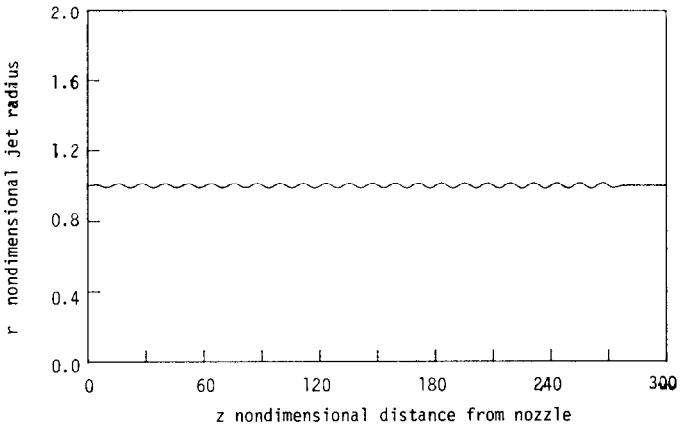

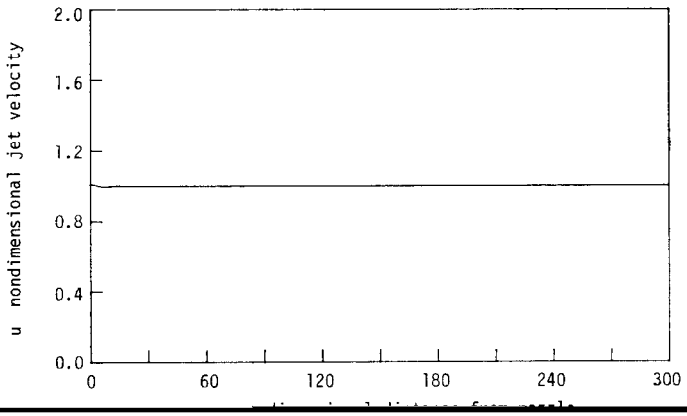

$p = 100$ ($k \approx 0.12$), $h = 0.5$, $t = 23$ input cycles.

The effect of viscosity on the growth rate of the disturbance has also been studied in the context of the Cosserat theory by Caulk and Naghdi [19].

6. Conclusions

Simultaneous numerical solution of the nonlinear Cosserat fluid jet equations is quite possible using several FD schemes. For the problem of a semi-infinite jet emanating from a nozzle with a harmonic excitation of the velocity at the nozzle and with the finest space-time lattice that was reasonable to use, good solutions were obtained.

The small-amplitude periodic perturbation of the velocity is transformed into a

wave, of the same wavelength, which grows in amplitude if the frequency, ω, is less than 1 until it finally breaks the jet at a specific point downstream. If $\omega > 1$ the disturbance is stable and therefore does not grow to break the jet. For the unstable frequencies the jet breakoff points, for various conditions, and the size of the main drops were accurately predicted compared to results of the perturbation solution of the same equations due to Bogy [2, 3] and experimental results due to Pimbley and Lee [8].

Faster jets (higher Weber numbers) are shown to break farther from the nozzle than slower jets. Disturbances with smaller amplitudes grow more slowly and break the jet farther from the nozzle. Higher viscosity makes the jet break farther from the nozzle until a point is reached where the higher viscosity makes the growth rate so small that for all practical purposes no jet breakup occurs.

While the disturbance is growing downstream the dimensionless axial velocity of the jet is shown to be nearly equal to the initial nominal value (deviates no more than $\pm 5\%$) but it very rapidly blows up as the breakoff point is approached. It is this behaviour of the velocity which causes most of the difficulties with the FD schemes at the breakoff region.

Formation of small satellite drops interspersed between the main drops is well predicted for the fast jets. However, with the schemes presented in this work and with the finest space-time mesh used the correct behaviour of these drops near breakoff as influenced by changing the amplitude of the nozzle excitation is not as well predicted as in the third perturbation solution of these equations by Bogy [3]. The solution obtained here is more similar to the second perturbation solution in Bogy [2].

ACKNOWLEDGMENT

This work was supported by IBM Research in San Jose, California, and by the Department of Mechanical Engineering, University of California, Berkeley.

REFERENCES

1. D. B. BOGY, *Phys. Fluids* **21**, No. 2 (1978), 190–197.
2. D. B. BOGY, *IBM J. Res. Develop.* **23**, No. 1 (1979), 87–92.
3. D. B. BOGY, *Phys. Fluids* **22**, No. 2 (1979), 224–230; **22** (1979).
4. D. B. BOGY, *J. Appl. Mech.* **45** (1978), 469–474.
5. D. B. BOGY, *Ann. Rev. Fluid Mech.* **11** (1979), 207–228.
6. A. E. GREEN, P. M. NAGHDI, AND M. L. WENNER, *Proc. Roy. Soc. London Ser. A* (1974), 337, 485–507.
7. A. E. GREEN, *Internat. J. Engrg. Sci.* **14** (1976), 49–63.
8. W. T. PIMBLEY, AND H. C. LEE, *IBM J. Res. Develop.* **21**, No. 1 (1977), 198–205.
9. S. D. CONTE, AND R. T. DAMES, *Math. Tables and Other Aids to Computation* **12** (1958), 198–205.
10. A. ILAN, *J. Comput. Phys.* **29** (1978), 389–403.
11. D. GOTTLIEB, AND E. TURKEL, *J. Comput. Phys.* **26** (1978), 181–196.
12. R. S. HIRSH, *J. Comput. Phys.* **19** (1975), 90–109.
13. Y. ADAM, *J. Comput. Phys.* **24** (1977), 10–22.

14. M. CIMENT, S. LEVENTHAL, AND R. WEIMBERG, *J. Comput. Phys.* **28** (1978), 135–166.
15. S. A. ORSZAG AND M. ISRAEL, *Ann. Rev. Fluid Mech.* **6** (1974), 281–318.
16. G. MORETTI AND M. SALAS, *J. Comput. Phys.* **5** (1970), 487–506.
17. C. W. HIRT, *J. Comput. Phys.* **2** (1968), 339–355.
18. R. H. MILLER, *J. Comput. Phys.* **2** (1967), 1–7.
19. D. A. CAULK AND P. M. NAGHDI, *J. Appl. Mech.* **46** (1979), 291–297.
20. S. J. SHINE, "Finite Difference Solution of the Nonlinear Cosserat Jet Equations for a Viscous Fluid with Surface Tension," Ph. D. dissertation, U.C. Berkeley, 1979.
21. D. A. CAULK AND P. M. NAGHDI, *Arch. Rational Mech. Anal.* **69** (1979), 1–30.